Available online at www.sciencedirect.com
SCIENCE DIRECT®
Surface Science 545 (2003) 70–84
SURFACE SCIENCE
www.elsevier.com/locate/susc

# Step structure and surface morphology of hydrogen-terminated silicon: (0 0 1) to (1 1 4)

A.R. Laracuente *, L.J. Whitman

*Naval Research Laboratory, Code 6177, 4555 Overlook Avenue SW, Washington, DC 20375-5342, USA*

Received 29 May 2003; accepted for publication 19 August 2003

**Abstract**

We have determined the equilibrium step structures and surface morphology for the whole range of monohydride-terminated (0 0 1)-terrace-plus-step silicon surfaces using scanning tunneling microscopy. The transformation in the equilibrium Si surface morphology caused by H-termination can be categorized into three different regimes delineated by the types of steps present on the clean surfaces. On nominal Si(0 0 1), the single-layer height B-type steps ($S_B$) are mostly non-rebonded and rougher after H passivation. On surfaces dominated by double-layer height B-type steps ($D_B$), such as Si(1 1 11), the non-rebonded $D_B$ and $S_B$ steps show a lower formation energy. Measurements on post-annealed surfaces indicate that the $D_B$ step formation energies strongly depend on H chemical potential. Smoother morphologies are observed following H-termination of surfaces oriented approximately between (1 1 7) and (1 1 4). This effect is quite apparent on Si(1 1 5), where the monohydride surface exhibits large (1 1 5)-(2×2) domains, a structure *not* observed on the clean surface. All of these structural modifications result directly from a change in the relative energies of the possible single- and double-layer step configurations.


*Keywords:* Scanning tunneling microscopy; Silicon; Single crystal surfaces; Hydrogen atom; Chemisorption; Surface structure, morphology, roughness, and topography; Surface energy; Equilibrium thermodynamics and statistical mechanics

## 1. Introduction

Surface steps are a fundamental building block in layer-by-layer film growth. It is well known that adsorbates can change the step edge structure and energetics, inducing morphological and structural changes. Upon adsorption, the surface chemical potential and surface free energy is altered, and the surface will restructure to lower its surface energy. Semiconductors are particularly susceptible to adsorbates and these kinds of changes [1]. Some surfaces will undertake extreme morphologies to assure a low-energy configuration. Roughening [2,3], faceting [4,5], growth mode modification [6,7], and surface reconstructions [8–10] are just a few of the properties that are directly tied to surface temperature and/or adsorbate coverage (i.e. chemical potential). Understanding how changes in chemical potential and surface free energy induced by adsorption affect the surface morphology and reconstruction is an interesting and important ongoing topic in surface science [11–15].

Because of its technological importance, silicon is the most widely studied semiconductor surface.

* Corresponding author. Tel.: +1-202-767-2519; fax: +1-202-767-3321.
*E-mail address:* laracuente@nrl.navy.mil (A.R. Laracuente).

0039-6028/$ - see front matter © 2003 Elsevier B.V. All rights reserved.
doi:10.1016/j.susc.2003.08.038

# Report Documentation Page

*Form Approved*
*OMB No. 0704-0188*



| 1. REPORT DATE | 2. REPORT TYPE | 3. DATES COVERED |
|---|---|---|
| **MAY 2003** | | **00-00-2003 to 00-00-2003** |

| 4. TITLE AND SUBTITLE | 5a. CONTRACT NUMBER |
|---|---|
| **Step structure and surface morphology of hydrogen-terminated silicon: (001) to (114)** | 5b. GRANT NUMBER |
| | 5c. PROGRAM ELEMENT NUMBER |
| 6. AUTHOR(S) | 5d. PROJECT NUMBER |
| | 5e. TASK NUMBER |
| | 5f. WORK UNIT NUMBER |
| 7. PERFORMING ORGANIZATION NAME(S) AND ADDRESS(ES) **Naval Research Laboratory,Code 6177,4555 Overlook Avenue SW,Washington,DC,20375** | 8. PERFORMING ORGANIZATION REPORT NUMBER |
| 9. SPONSORING/MONITORING AGENCY NAME(S) AND ADDRESS(ES) | 10. SPONSOR/MONITOR'S ACRONYM(S) |
| | 11. SPONSOR/MONITOR'S REPORT NUMBER(S) |

12. DISTRIBUTION/AVAILABILITY STATEMENT
**Approved for public release; distribution unlimited**

13. SUPPLEMENTARY NOTES

14. ABSTRACT

**We have determined the equilibrium step structures and surface morphology for the whole range of monohydride-terminated (0 0 1)-terrace-plus-step silicon surfaces using scanning tunneling microscopy. The transformation in the equilibrium Si surface morphology caused by H-termination can be categorized into three different regimes delineated by the types of steps present on the clean surfaces. On nominal Si(0 0 1),the single-layer height B-type steps (SB) are mostly non-rebonded and rougher after H passivation. On surfaces dominated by double-layer height B-type steps (DB),such as Si(1 1 11),the non-rebonded DB and SB steps show a lower formation energy. Measurements on post-annealed surfaces indicate that the DB step formation energies strongly depend on H chemical potential. Smoother morphologies are observed following H-termination of surfaces oriented approximately between (1 1 7) and (1 1 4). This effect is quite apparent on Si(1 1 5),where the monohydride surface exhibits large (1 1 5)-(2 · 2) domains,a structure not observed on the clean surface. All of these structural modifications result directly from a change in the relative energies of the possible single- and double-layer step configurations.**

15. SUBJECT TERMS

| 16. SECURITY CLASSIFICATION OF: | | | 17. LIMITATION OF ABSTRACT | 18. NUMBER OF PAGES | 19a. NAME OF RESPONSIBLE PERSON |
|---|---|---|---|---|---|
| a. REPORT **unclassified** | b. ABSTRACT **unclassified** | c. THIS PAGE **unclassified** | **Same as Report (SAR)** | **15** | |

Although the surface morphologies and reconstructions on clean Si surfaces with a wide range of crystallographic orientations have been examined, most studies have concentrated on orientations near (0 0 1) [16,17]. In the vicinity of (0 0 1), surfaces are described as having an (0 0 1)-like terrace-plus-step morphology [16]. Steps are labeled according to their height (single- (S) vs. double-layer (D) height) and to the dimer orientation on the terrace preceding the step (A- vs. B-type) [18]. Adsorption on Si can produce many different changes to the surface morphology. Surface faceting and new reconstructions are just a few of these changes.

Hydrogen is one of the simplest and most important adsorbates on Si. Particular attention has been paid to its adsorption on nominal Si(0 0 1) [19,20]. Saturation exposure to molecular $H_2$ at room temperature simply passivates the steps [21–24]. While adsorption at very-high temperatures and pressures produces a monohydride surface [25], these exposure conditions are far from ideal. Instead, atomic hydrogen, rather than molecular $H_2$, is used to prepare a well ordered, low defect density H-terminated surface. The morphology and reconstruction after passivation strongly depends on the H chemical potential [26]. By selecting adequate surface temperature and exposure conditions, a $(1\times1)$, $(3\times1)$, or $(2\times1)$ surface is prepared [20,27–30]. In the case of low temperature exposures, Si is etched primarily by the evolution of $SiH_4$ from $SiH_{x=2,3}$ hydrides [29]. Because these hydride species are unstable above 550 K, the monohydride surface prepared between 600 and 675 K is impervious to etching [31]. Although adsorption of H on Si has been well studied, we have recently found that H changes the atomic structure of the steps and that these changes can affect the surface morphology on Si(0 0 1) vicinal surfaces [32]. Here we report the surface morphology of monohydride-terminated Si and the changes induced by H for the whole range of surface orientations from (0 0 1) to (1 1 4).

## 2. Experimental

The experiments were performed in ultra-high vacuum (UHV) using commercially available Si wafers oriented within 0.5° of (0 0 1), (1 1 11), (1 1 7), (1 1 5), and (1 1 4). Samples were cut from a wafer, transferred into the UHV chamber, and degassed for 8 h. A clean Si surface was prepared by heating the sample twice at 1500 K for 1 min and then 5 s, consecutively, while maintaining the pressure in the UHV chamber below $8\times10^{-10}$ Torr. The sample cools radiatively to room temperature after each heating, and there is a minimum 5-min delay between each heating. Samples were cleaned many times using the same procedure without affecting the apparent cleanliness of the surface or the long- and short-range order. Monohydride-terminated surfaces were prepared by exposing clean samples to atomic H while heating the sample at 615 K. Atomic H was produced by decomposing molecular $H_2$ with a hot tungsten filament located 1 cm away from the sample. After H exposure some samples were post-annealed at the same dosing temperature. Filled and empty state scanning tunneling microscope (STM) images of the clean and monohydride surfaces were collected at 2 V and 0.1 nA.

## 3. Results

Before describing our results on the monohydride surface, it is useful to review the clean surface. The studied surfaces belong to a family of surfaces having an (0 0 1)-terrace-plus-step morphology [16]. In this family (0 0 1) and (1 1 4) (19.5° away from (0 0 1) towards (1 1 1)) [33] are the only stable, low-energy planes. The other orientations can be sorted into four regions depending on the kinds of steps present at the surface. Fig. 1 shows the distribution of the steps as a function of miscut angle in the four regions. Region I consists of alternating single-layer A- and B-type steps ($S_A$ and $S_B$), whereas region III is composed solely of rebonded double-layer steps (r-$D_B$). Surfaces in regions II and IV contain a mixture of steps; $S_A + S_B$ mixed with r-$D_B$ in region II, and non-rebonded $D_B$ steps (n-$D_B$) mixed with r-$D_B$ in region IV. Note that in this region the ratio of n- to r-$D_B$ steps increases from zero on (1 1 7) to one on Si(1 1 4). To help the reader visualize the different step structures referred to in this work, top and

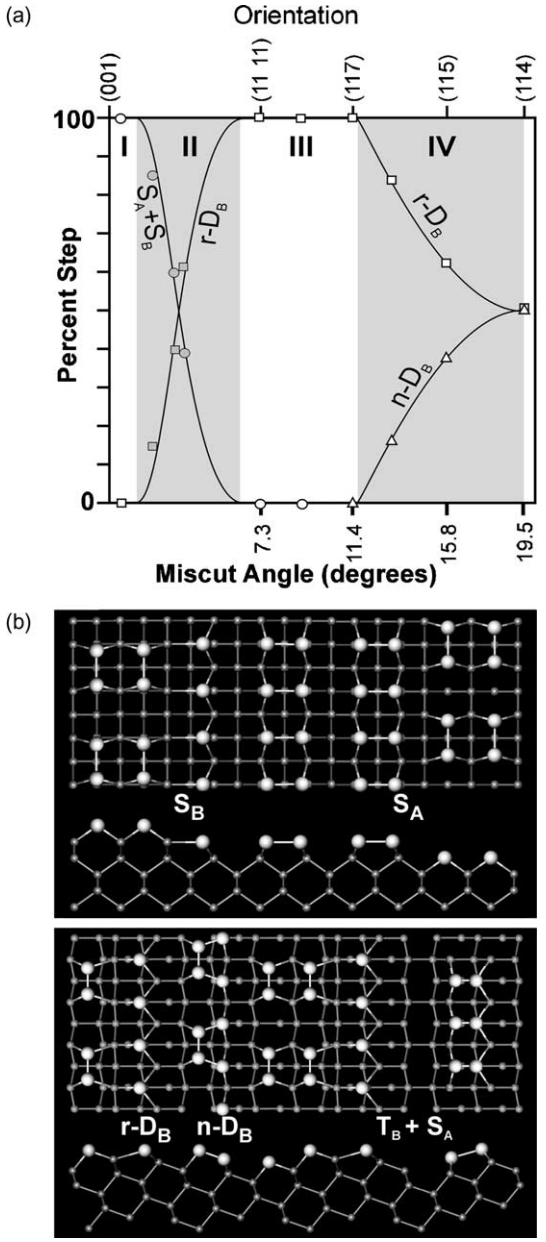


Fig. 1. Distribution of single- and double-layer steps as a function of miscut angle on clean vicinal Si(0 0 1). (a) The type of steps present on the surface can be categorized into four regions: (I) $S_A + S_B$ steps, (II) $S_A + S_B$ mixed with r-$D_B$ steps, (III) r-$D_B$ steps, and (IV) r-$D_B$ blend with n-$D_B$ steps. The data points shown in region II, filled circles and squares, were taken from Ref. [17]. (b) Structural models (top and side views) of the most common steps found on clean and H-terminated vicinal Si(0 0 1). The triple layer-height type B step ($T_B$) is only found on the H-terminated surfaces.

side view ball and stick models of the step structures are also shown in Fig. 1.

To illustrate how the steps appear at the atomic scale, high-resolution STM images of the clean (0 0 1)-like surfaces are depicted in Fig. 2. On $S_A$ steps, the dimer rows of the upper terrace are oriented parallel to the step edge, whereas on $S_B$ steps they are oriented perpendicular to the step edge. Most $S_B$ steps on the clean surface are rebonded, meaning that there is an extra row of atoms adjacent to the step edge. These atoms are clearly visible as a 1× row of protrusions next to the step edge (Fig. 2(b)). Structurally, r-$D_B$ steps are very similar to $S_B$ steps, a dimer followed by a pair of rebonded atoms. The brightness of the rebonded atom relative to the dimer depends on the miscut angle. For instance, on Si(1 1 11) the protrusions associated with the dimers are much brighter than the protrusions associated with the rebonded atoms (Fig. 2(c)). In contrast, on Si(1 1 4) the dimer is hardly visible while the rebonded atom is the brightest feature in the images (Fig. 2(d)). The appearance of the n-$D_B$ steps in the STM images depends on the miscut angle. On

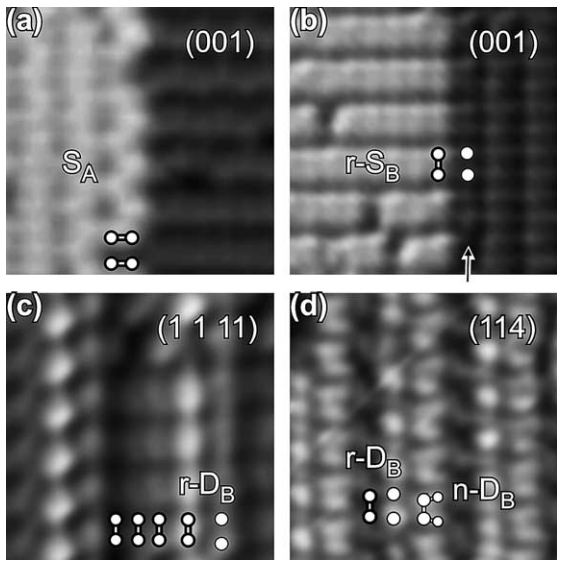


Fig. 2. 5 nm×5 nm filled-state STM images of clean (a, b) Si(0 0 1), (c) (1 1 11), and (d) (1 1 4). Models are overlaid in the figure to highlight the various step structures. (b) A row of rebonded atoms is indicated with an arrow.

Si(1 1 5), the STM simply images the dimer at the step edge (not shown). At larger angles, like Si(1 1 4), the STM images the bonds between the dimer and the step edge atoms. This shows up as a 2× feature of oblong protrusions running perpendicular to the step edge. Independent of sample orientation, all the steps have a unique appearance on the STM images, making it possible to quantify the step structures on clean, vicinal (0 0 1) surfaces.

To appreciate the morphological changes produced by the passivation process, STM images of clean and monohydride-terminated Si at various orientations are depicted in Fig. 3. First, we consider the morphology of the clean surfaces (left column). On the well-known (0 0 1) surface, alternating $S_A$ and $S_B$ steps are easily identified in the figure. Surfaces in region III, like (1 1 11) and (1 1 7), have a unit cell composed of *n*-dimers plus one r-$D_B$ step, with *n* typically between 3 and 8. This type of unit cell produces a row-like structure oriented along the $[\bar{1}\,1\,0]$ direction. The frequency of the $D_B$ steps increases with increasing miscut angle, reaching a maximum at Si(1 1 7). It should be noted that wafer terrace steps, indicated in Fig. 3(c) and (e), will be ignored in this work. In region IV, which includes Si(1 1 5), the surface morphology is best described by a periodic array of nanoscale facets whose sides are (1 1 7)- and (1 1 4)-oriented. A (1 1 5)-oriented segment connects the facets together. The surface morphology of Si(1 1 4) is very similar to that of nominal Si(0 0 1), where large (1 1 4) terraces are separated by terrace-steps.

Moving ahead to the effects of H on Si, H-terminated Si(0 0 1) and H-terminated Si(1 1 4) appear to be unaltered after H-passivation (see Fig. 3(f) and (j)). On monohydride Si(0 0 1), a large number of kinks at the $S_B$ step edge are observed. In general, these two surfaces still exhibit the typical terrace-plus-step morphology. In contrast, the surface morphology of (1 1 11), (1 1 7), and (1 1 5) is different after H exposure. Si(1 1 11) and Si(1 1 7) have become disordered, with the degree of atomic-scale disorder highest on Si(1 1 7). Only a hint of the typical $[\bar{1}\,1\,0]$ row-like structure remains for these two orientations. Quite the opposite, Si(1 1 5) appears to be *flatter* overall after H exposure. Although nanofacets remain visible,

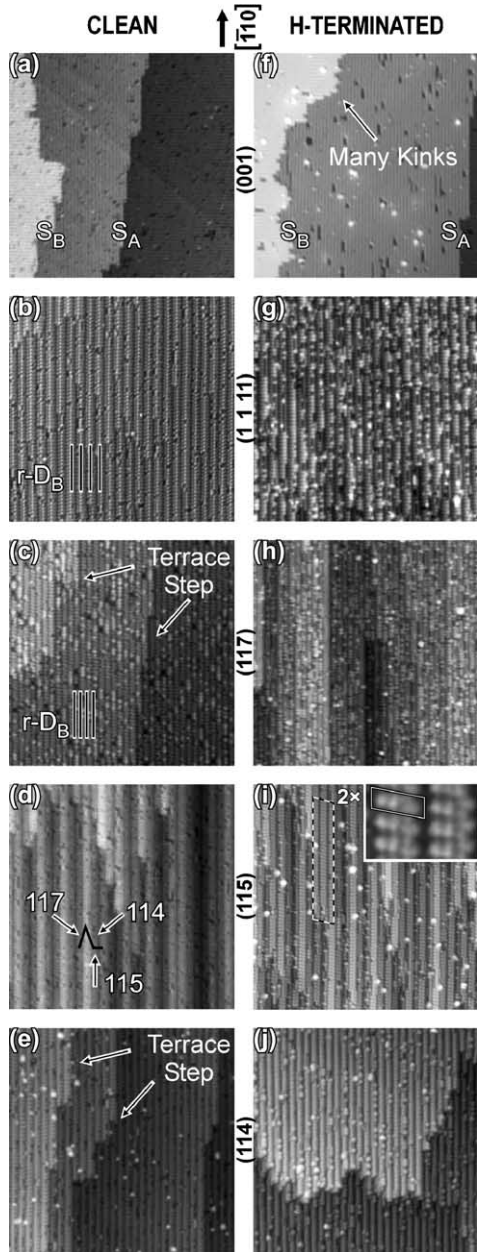


Fig. 3. 50 nm × 50 nm filled-state STM images of clean and monohydride-terminated Si(0 0 1), (1 1 11), (1 1 7), (1 1 5), and (1 1 4). (b and c) The spacing between r-$D_B$ steps is highlighted with vertical lines. (c and e) Terrace steps are indicated with arrows. (d) On a typical Si(1 1 5) nanofacet, the facet segments are oriented in the (1 1 7), (1 1 4), and (1 1 5) as indicated with the arrows. (i) A 2× domain observed in the H-terminated Si(1 1 5) surface is highlighted. A close up view of the domain is shown in the inset.

some areas of the surface now have an ordered, planar 2× (1 1 5) structure that extends over areas as large as 2 nm×25 nm (inset Fig. 3(i)).

The change in surface morphology is directly related to the structure of the steps. To show the effect of H exposure on the steps, high-resolution STM images of the monohydride-terminated steps are shown in Fig. 4. A general feature of passivating a surface with H is that the dimer is no longer buckled [20]. Aside from that, H has no obvious effect on the structure of $S_A$ steps. In contrast, the structure of the $S_B$ steps changes after H exposure. Most noticeable is the absence of the rebonded atoms that occur next to the step edge on the clean surface, indicating that the H-terminated steps are now non-rebonded (n-$S_B$) steps. A pronounced change in structure is observed in Si(1 1 11), where a mixture of step structures now

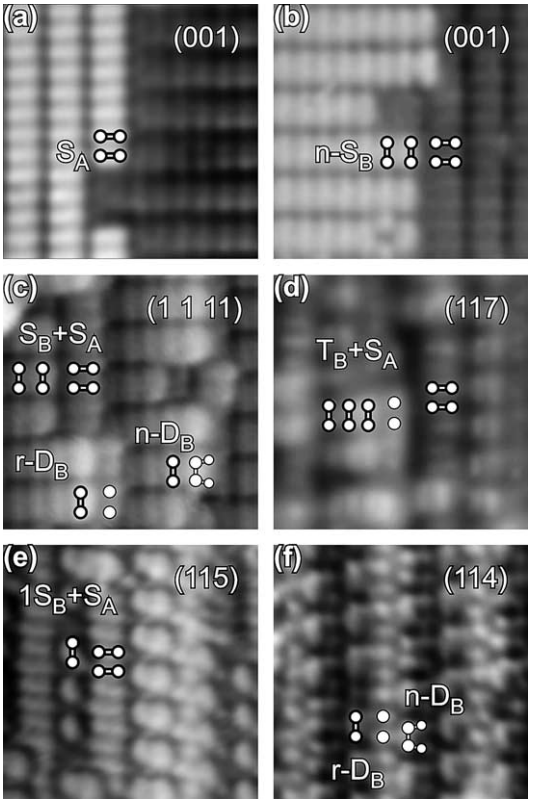


Fig. 4. 5 nm×5 nm STM images of monohydride-terminated Si (0 0 1), (1 1 11), (1 1 7), (1 1 5), and (1 1 4). Overlaid models are use to highlight the structure of the steps.

decorates the surface. Among the different step structures, the most striking is the $S_A + S_B$ step combination (produced by the splitting of $D_B$ steps), with the $S_B$ step being n-$S_B$ like on H-terminated Si(0 0 1). Furthermore, r-$D_B$ and n-$D_B$ steps coexist on this surface. There are two additional step structures found on both Si(1 1 7) and Si(1 1 5). The first one is a triple-layer high type B step ($T_B$) followed by an $S_A$ step ($T_B + S_A$). The second new step structure consists of a single-dimer-wide $S_B$ step followed by an $S_A$ step, labeled $1S_B + S_A$. Under certain conditions H has little effect on Si(1 1 4), and a nearly perfect H-terminated surface can be prepared with step structures that are unchanged. It is worth noting that the H-terminated n-$D_B$ steps have a very different appearance compared to the clean surface. On the H-terminated n-$D_B$ steps, the step edge atoms are clearly visible as round protrusions with a 1× period. As in the case on the clean surfaces, all the different step structures have a unique appearance on the H-terminated surfaces.

Because of spatial changes in the electronic structure as a function of miscut angle, the appearance of r-$D_B$ and n-$D_B$ on H-terminated surfaces are somewhat orientation dependent. Dual-bias STM images offer the best method to observe these changes and to spot features not usually observed in filled-state images. Fig. 5 depicts empty-state images of Si(0 0 1) and (1 1 4), and dual-bias STM images of H-terminated Si(1 1 11) and (1 1 5). Whereas the dimers on Si(0 0 1) and (1 1 4) are unbuckled, the rebonded atoms on Si(1 1 4) are slightly buckled (indicated by the alternating intensity of the rebonded atoms). In contrast, dimers on Si(1 1 11) and Si(1 1 5) show a substantial buckling in the empty state images. In addition, a very interesting feature is observed on Si(1 1 11). A row of small protrusions with a 1× periodicity emerge between the last two dimers of the n-$D_B$ step edge (highlighted with open circles in the figure). This feature, not observed in the r-$D_B$ steps, indicates that there must be some type of rehybridization of the bonding at the step. (Although the specific structural origin of this effect is not yet known, it is distinctly and reproducibly observed.) On Si(1 1 5), the rebonded atoms are distinctively observed as a row of 1× protrusions in the empty state images. Because of

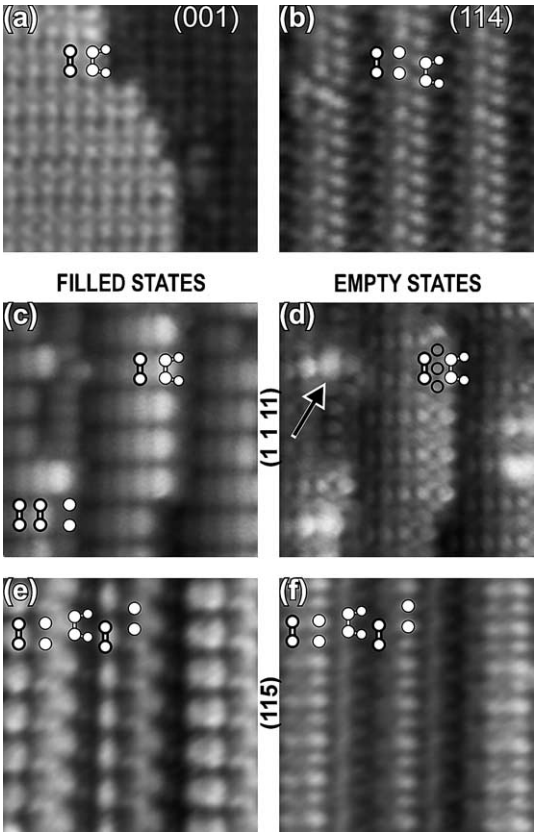


Fig. 5. (a and b) Empty state STM images, 5 nm on the side, of monohydride Si(0 0 1) and (1 1 4). (c–f) 5 nm × 5 nm filled and empty states STM images of H-terminated Si(1 1 11) and Si(1 1 5). Overlaid models highlight a few of the steps. (d) An arrow points to the location of a r-$D_B$ step, while open circles highlight an interesting feature that only appears between dimers near the step edge.

the larger miscut angle on Si(1 1 5), the step edge atoms at the n-$D_B$ steps are now visible. The dimers at the n-$D_B$ step show up as a diffuse row in the empty state image.

An interesting question is the fate of the rebonded atoms on Si(0 0 1), which are missing from the $S_B$ steps after H-termination. A meticulous inspection of the surface revealed something fascinating: when the sample temperature was quenched to room temperature after H exposure, while maintaining a constant $H_2$ pressure, string-like rows (highlighted with an arrow in the Fig. 6(a)) appeared a few dimers away from the step edge. These features appear on the surface independent

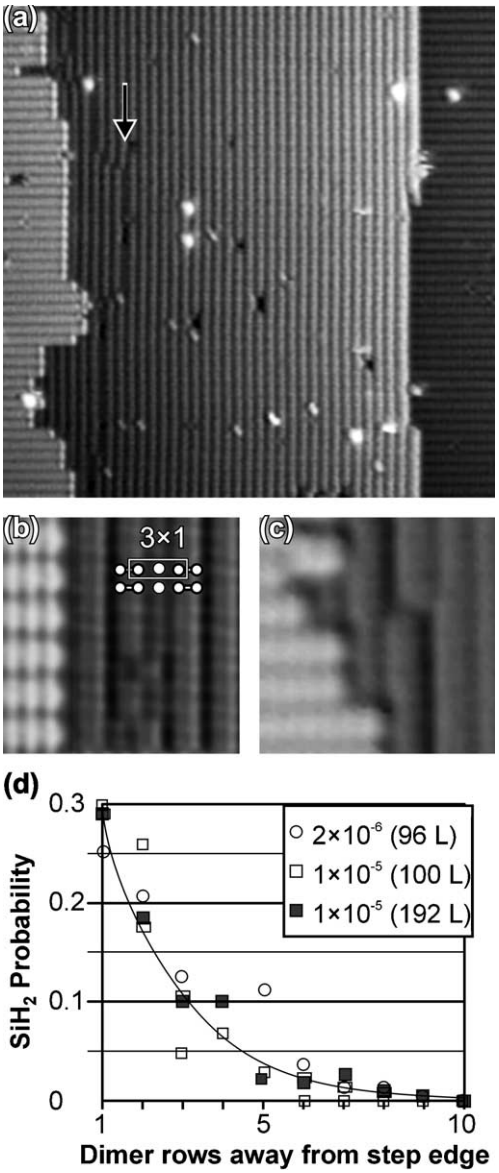


Fig. 6. STM images, 35 nm × 35 nm (a) and 5 nm × 5 nm (b and c), of monohydride-terminated Si(0 0 1). (a) The arrow points to a string feature that is observed on this surface under specific exposure conditions. (b) A model is overlaid on the string feature to highlight its 3×1 character. (c) Same surface as (b) that has been post-annealed for 10 min at 600 K. (d) Probability of finding $SiH_2$ (1×1 feature) as a function of the number of dimer rows away from the step edge. The line is an exponential fit to the average of the data.

of $H_2$ pressure, and are not observed near the $S_A$ steps. Each structure is made out of a 1× row of

protrusions inserted between dimer rows, resulting in a local $3\times1$ reconstruction (Fig. 6(b)). This local reconstruction is typical of a dihydride phase [34,35], in which the dihydride units are adjacent to monohydride-terminated dimers. The probability of finding a dihydride several dimer rows away from the step edge is shown in the figure. When the sample is post-annealed after H exposure at the same passivation temperature but without any background $H_2$ pressure, a trench like feature is observed on the surface (Fig. 6(c)). The region around the trench still has a local $3\times$ reconstruction, but with a row of vacancies inserted between dimer rows; the dihydrides have been replaced with vacancies. These observations are related to the disappearance of the rebounded atoms, and their relation will be address later in the paper.

In order to investigate what role the H chemical potential ($\mu_H$) plays during the passivation process, H-terminated Si(1 1 11) was studied as a function of $H_2$ background pressure, exposure time, and post-annealing time. The results are summarized in Fig. 7. First, we consider the effects that exposure time has on the structure of the steps (Fig. 7(a)–(c)). These surfaces were exposed for 2, 6, and 10 min at a constant $H_2$ background pressure of $2\times10^{-6}$ Torr and were cooled to room temperature before pumping away the $H_2$ (no post-annealing). Two minutes of H exposure produced a surface that is no longer exclusively composed of r-$D_B$ steps. Instead, the surface is made of a mixture of r-$D_B$, n-$D_B$ and $S_A+S_B$ steps. Six minutes exposure increased the $S_A+S_B$ step concentration and dramatically decreased the number r-$D_B$ steps. In contrast, further exposure (10 min) had almost no effect on the step concentrations. The most significant difference between the 6 and 10 min exposures is that the $S_A+S_B$ steps and n-$D_B$ steps have formed small domains. Although the surface morphology after 2, 6, and 10 min is very similar, the coverage of $S_A+S_B$ steps is significantly different after 2 and 6 min of exposure. The $S_A+S_B$ step concentration as a function of dose is plotted in Fig. 7(d).

Next, we consider the role of the $H_2$ background pressure during the passivation process. Si(1 1 11) was exposed to $2\times10^{-6}$ and $1\times10^{-5}$ Torr $H_2$ without post-annealing (see Fig. 7(c) and (e), respectively). The length of the exposure was adjusted such that these two surfaces were exposed to a similar amount of $H_2$. However, the results are dramatically different. The most significant difference is the presence of $D_A$ steps after the $1\times10^{-5}$ Torr $H_2$ exposure, a step structure that is *never* observed on vicinal Si(0 0 1) surfaces. A few $S_A+S_B$ and n-$D_B$ steps are also observed on the surface, but the r-$D_B$ step structure is not observed. Finally, we consider the role of post-annealing a H-terminated surface without the presence of background $H_2$. Fig. 7(f) depicts the surface shown in Fig. 7(c) after it had been post-annealed for 390 min. About

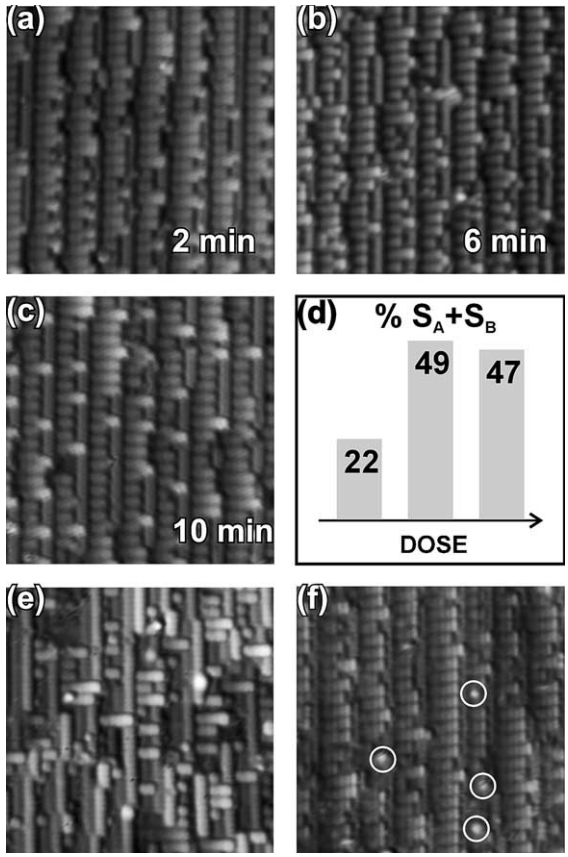


Fig. 7. Surface morphology of monohydride-terminated Si(1 1 11) produced at a background of $2\times10^{-6}$ Torr $H_2$ and exposed for (a) 2 min, (b) 6 min, and (c) 10 min. (d) A plot of the $S_A+S_B$ step distribution of each of the previous surfaces. (e) Surface exposed to $1\times10^{-5}$ Torr $H_2$ for 2 min. (f) The same surface that is depicted on (c) but post-annealed for 390 min at 600 K. Dangling bonds are highlighted with open circles.

15% of the surface is covered with bright protrusions which are attributed to dangling bond due to H desorption. In sharp contrast to the previous surfaces, this surface is mostly composed of r-$D_B$ steps (7% $S_A + S_B$ and 6% n-$D_B$).

In addition to changing the atomic-scale structure of the steps, H adsorption also alters the large-scale morphology of Si surfaces. STM images of hydrogen-terminated Si(1 1 5) prepared under five different H exposure conditions are depicted in Fig. 8. Exposure at a background pressure of $6\times10^{-6}$ Torr $H_2$ and a surface temperature of 600 K (Fig. 8(c)) appeared to have no obvious effect on the surface morphology. The typical nanofacet morphology observed on the clean surface (Fig. 2(d)) is still visible on this surface, but the surface is not well ordered at the atomic scale. Similarly, surfaces prepared at a lower pressure exposure (Fig. 8(d)) exhibit a disordered, nanofaceted surface. In contrast, at a higher $H_2$ pressure (Fig. 8(a)) and surface temperatures 40 degrees below and above 600 K (Fig. 8(e) and (b) respectively) the nanofacet morphology is no longer present and the surface is very disordered.

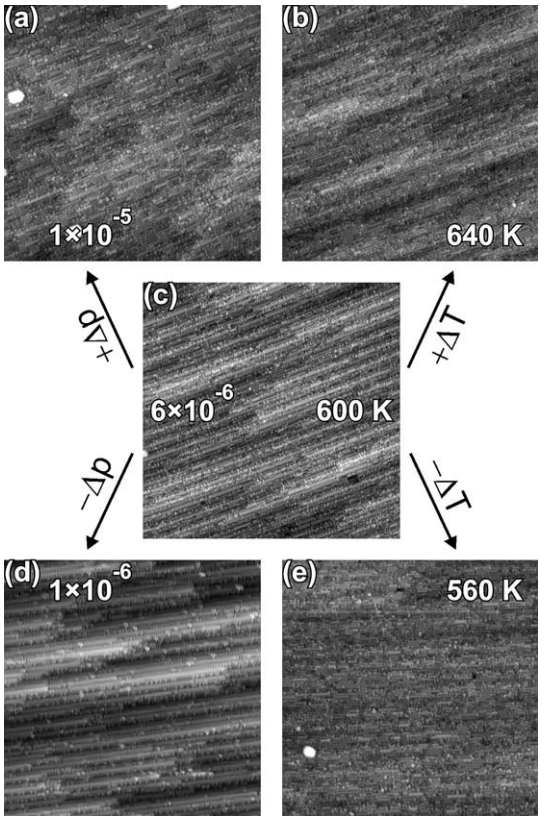


Fig. 8. STM images, 100 nm × 100 nm, of hydrogen-terminated Si(1 1 5) prepared at various exposure conditions to show the effects of $H_2$ pressure and surface temperature: 600 K and (a) $1\times10^{-5}$ Torr $H_2$, (c) $6\times10^{-6}$ Torr $H_2$, (d) $1\times10^{-6}$ Torr $H_2$, and $6\times10^{-6}$ $H_2$, and (b) 640 K, (e) 560 K.

## 4. Discussion

### 4.1. Etching

It is important to determine if the changes caused by H adsorption on Si(0 0 1) vicinals are the result of surface etching. Previous work has clearly established that etching—which primarily takes place by the evolution of $SiH_4$ from $SiH_{x=2,3}$ hydrides—should not happen at the surface temperatures used in this study where these hydrides are not stable [29,31]. Nevertheless, we have carefully examined this possibility, looking for signs of etching on the (0 0 1)-like terraces and at the step edges.

On nominal Si(0 0 1), the only evidence of etching we observed is associated with the removal of the single row of rebonded atoms along the $S_B$ step edge (Fig. 6). Recall that $S_B$ steps change their structure from r-$S_B$ to n-$S_B$ after H passivation. This structural transformation requires the removal of the rebonded atoms from the r-$S_B$ step. To our surprise, when the surface is radiatively cooled to room temperature under a $H_2$ background pressure after passivation, about 80% of the rebonded atoms remain on the surface. The formerly rebonded atoms remain on the surface as a single row of protrusions between dimer rows, creating a local $3\times1$ reconstruction, indicative of $SiH_2$. If the surface is instead post-annealed without $H_2$ present, i.e. at a lower H chemical potential, $SiH_2$ apparently becomes unstable and desorbs from the surface, leaving behind the observed vacancy defect (Fig. 6(c)). This is the only type of terrace etching that is ever observed on nominal Si(0 0 1), and to our knowledge has not been previously reported. It is constant in amount, 2 Si atoms per $S_B$ step or $1.41\tan(\theta)$ ML, where $\theta$ is the miscut angle. Once $SiH_2$ desorbs, etching stops.

The removal of the $SiH_2$ appears to be consistent with the mechanism proposed by Gates et al. 14 years ago [29], whereby adjacent $SiH_2$ recombine to desorb as $Si_2H_2$. Based on temperature program desorption, they hypothesized that the $Si_xH_y$ products coincident with the $\beta_2$-$H_2$ state originated from desorbing $Si_2H_2$. But, they also acknowledged that Si and SiH desorption could also account for their results. Our STM results clearly establish that the disappearance of the $SiH_2$ species does not generate any dangling bonds, as would occur if $SiH_4$ or $Si_2H_4$ desorbed. Therefore, the vacancies must originate from the concerted desorption of $Si_2H_2$.

The question of etching on Si(1 1 11) is more complex. At a first glance, it appears that the restructuring of the r-$D_B$ steps into $S_A + S_B$ steps may be the work of terrace etching; the dimer at the r-$D_B$ step is etched away, exposing an $S_A$ step. Although this could explain the emergence of $S_A + S_B$ steps, it is not consistent with the fact that the coverage of $S_A + S_B$ steps remained constant after 6 min of H exposure. This fact would imply that etching must stop after 6 min, which seems very unlikely. In addition, features that are commonly attributed to surface etching, like terraces becoming filled with vacancies and pits, or steps becoming rougher with longer exposures, are never observed on any of the surfaces [36–40]. Therefore, we conclude that, in general, etching is not the source of the morphological and structural changes observed on vicinal Si(0 0 1) surfaces. Rather, the changes are caused by surface diffusion (which will be addressed later in the paper).

### 4.2. Local equilibrium

Another important issue is whether the surfaces have reached equilibrium or not. A surface can be assumed to be in local equilibrium if a measurement does not change with time or further exposure. For instance, on nominal Si(0 0 1), hydrogen promotes the formation of many kinks without significantly altering the overall surface morphology. To determine whether this structure is the equilibrium morphology, we analyzed the probabilities of having no kinks ($n_0$) and kinks of length $\pm r$ ($n_{\pm r}$) along the step edge. The kink probabilities on a clean surface are significantly different from that of a monohydride surface exposed to 120 L $H_2$. However, doubling the H-exposure (240 L) did not produce a significant change in the kink probabilities, suggesting that the steps have reached a local equilibrium. Similarly, the $S_A + S_B$ step coverage on Si(1 1 11) was analyzed as a function of H exposure. Under a constant $H_2$ background pressure of $2\times10^{-6}$ Torr, the $S_A + S_B$ step coverage increased from 0% to 49% during the first 6 min and remained constant after 10 min exposure. Because the $S_A + S_B$ steps did not change after 6 min, it is reasonable to assume that this surface has also attained a local equilibrium.

### 4.3. Surface diffusion

Given that there is no evidence for surface etching during H passivation, the structural changes must therefore be caused by diffusion-mediated mass transport. Rebonded atoms and dimers are the two basic structural units that can readily diffuse on the surface. As illustrated in Fig. 9, their diffusion will make specific type of step structures that one can compare to the step structures observed on the surface. We first examine the diffusion of rebonded atoms. Previously, Norton and coworker [41], observed that a small number of rebonded atoms diffuse away from the step edge at 400 K. As discussed above, on nominal Si(0 0 1) the rebonded atoms are passivated with two H atoms (dihydride), and 80% diffuse away from the step edge where they appeared to be stable. There is no trace of the other 20% of rebonded atoms in the form of vacancies or $SiH_2$. The "missing" atoms can be accounted for if they diffuse to a neighboring r-$S_B$ step and create two n-$S_B$ steps. Similarly, the diffusion of rebounded atoms on surface orientations with r-$D_B$ steps is illustrated in Fig. 9(b), where two rebonded atoms diffuse to a neighboring r-$D_B$ step creating a n-$D_B$ and a $S_B + S_A$ step. Note, however, that this requires the creation of a double-layer kink, and that there are no double-layer kinks on these surfaces, indicating that this mechanism is not energetically favored. Therefore, the changes observed after H exposure must then arise from dimer diffusion.

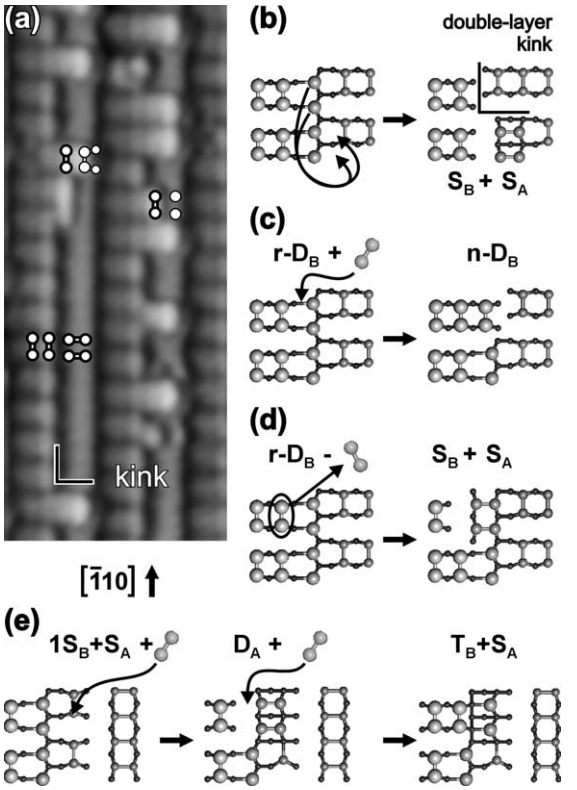


Fig. 9. (a) High resolution STM image of the Si(1 1 11) surface after 10 min of H exposure. Although the step structure has changed, the step edge remains straight. (b) Diffusion of rebonded atoms to a r-$D_B$ step will create a double-layer kink on the step edge. (c–e) Three possible scenarios that can account for the distribution of steps on H-terminated surfaces and avoid the formation of kinks. (c) Recombination of an adsorbed dimer with a r-$D_B$ step at the rebonded atoms site producing a n-$D_B$ step. (d) Dimer diffusion away from a r-$D_B$ step generates a "free" adsorbed dimer plus a $S_A + S_B$ step ($1S_A + S_B$ on Si(1 1 7) and higher orientations). (e) Adsorption of a free dimer at the dimer site of a $1S_B + S_A$ step generates a $D_A$ step. Similarly, adsorption at the $D_A$ step yields a $T_B + S_A$ step.

On nominal Si(0 0 1), the step edge dimers diffuse along the step edge, creating more kinks and significantly reducing the steric repulsion between neighboring dimers. On $D_B$-stepped orientations, dimers can either attach (Fig. 9(c)) or detach from r-$D_B$ steps (Fig. 9(d)), creating n-$D_B$ steps and $S_B + S_A$ steps, respectively. On Si(1 1 7) and Si(1 1 5) the $S_B$ steps are only one dimer wide (labeled the $1S_B + S_A$), and are the precursors to $T_B + S_A$ steps. Adsorption of a dimer at the $1S_B + S_A$ step creates a $D_A$ step, which upon sequential dimer adsorption creates he $T_B + S_A$ step. It is important to note that this mechanism preserves the row-like periodicity and is consistent with all step structures that are observed on these surfaces. Although there are many possible ways to rearrange the atoms, the arrangement must produce step structures that are consistent with the experiment. Therefore, we believe dimer diffusion along the step edges is responsible for nearly all morphological changes caused by H exposure.

### 4.4. Step energetics

The step energetics are ultimately responsible for a particular distribution of steps on a surface. We used two approaches to analyze the distribution of steps. On nominal Si(0 0 1), we analyzed the shape of the steps using the terrace-step-kink model of Burton, Cabrera, and Frank (BCF) [42–44]. Unfortunately, BCF failed to account for the kink distribution on monohydride-terminated Si(0 0 1) [32]. Below we discuss several possible explanations for this failure. In our second approach, we used Maxwell–Boltzmann (MB) statistics to determine the relative energies of the various step structures.

#### 4.4.1. Terrace-step-kink model

Within the BCF framework, the first- and second-nearest neighbor interaction potentials, $\phi_1$ and $\phi_2$ can be determined from the full kink probability distribution along a step, as follows:

$$\frac{\phi_1}{k_B T} = -\ln\left(\frac{n_{+1}n_{-1}}{n_0^2}\right), \tag{1}$$

$$\ln\left(\frac{n_{\pm r}}{n_0}\right) = r\left(\ln\frac{n_{\pm 1}}{n_0} - \frac{\phi_2}{k_B T}\right) + \frac{\phi_2}{k_B T}, \tag{2}$$

where $n_{\pm r}$ is the probability that at any given position along the step edge there is a positive or negative kink of length $r$. (Note that $q = n_0$ is often used in the literature to denote the probability of not having a kink along the step edge.) It follows that the formation energy of an *A-type* step is determined by the interaction energies across a *B-type* step, $\varepsilon_A = \phi_1^B/4 + \phi_2/2$, and vice-versa. Inherent to the symmetry in BCF, $\phi_2^A = \phi_2^B$; however on the H-terminated surface we found experimentally

that $\phi_2^A \neq \phi_2^B$ [32]. This asymmetry suggests that other interactions not accounted for in BCF must be considered.

To investigate possible interactions that could cause the asymmetry in $\phi_2$, we examined the probability of having a kink of length $i$ adjacent to a kink of length $j$; $P(i,j) = n_{\pm r=i}(x) \times n_{\pm r=j}(x+1)$. The pair probabilities $P(i,j)$, and their corresponding uncorrelated product $P(i) \times P(j)$, on the clean and H-terminated $S_A$ and $S_B$ steps are shown in Table 1. $P(i,j)$ were determined by counting the number of times a kink of length $i$ is followed by kink of length $j$ and dividing that number by the total number of units along the step. Note that we find $P(i,j)$ to be symmetric, $P(i,j) = P(j,i)$. On clean Si, $P(i,j)$ is uncorrelated, so that the probability at any point along the step is independent of its position. Clearly, this is not the case on H-terminated Si. For instance, for a H-terminated $S_B$ step, $P(1,1)$ and $P(1,-1)$ are not given by the uncorrelated probabilities $P(1)P(1)$ and $P(1)P(-1)$, respectively. This analysis shows that

Table 1
Measured pair probabilities $P(i,j)$ and the corresponding uncorrelated probability $P(i) \times P(j)$ for the clean and monohydride $S_A$ and $S_B$ steps. The value of $P(i)$ is simply the square root of $P(i) \times P(j=i)$. Cases where the pair probability is correlated, $P(i,j) \neq P(i) \times P(j)$, are highlighted in bold

| $i$, $j$ | $S_A$ step | | $S_B$ step | |
|---|---|---|---|---|
| | $P(i,j)$ | $P(i) \times P(j)$ | $P(i,j)$ | $P(i) \times P(j)$ |
| *Clean* | | | | |
| 0, 0 | 0.766 | 0.765 | 0.447 | 0.436 |
| 0, 1 | 0.062 | 0.062 | 0.075 | 0.078 |
| 0, 2 | 0.023 | 0.021 | 0.033 | 0.032 |
| 0, −1 | 0.016 | 0.019 | 0.052 | 0.059 |
| 0, −2 | 0.002 | 0.002 | 0.023 | 0.023 |
| 1, 1 | 0.004 | 0.005 | 0.014 | 0.014 |
| 1, 2 | 0.002 | 0.002 | 0.009 | 0.006 |
| 1, −1 | | | 0.016 | 0.011 |
| 1, −2 | | | 0.003 | 0.004 |
| *Monohydride* | | | | |
| 0, 0 | 0.664 | 0.637 | 0.096 | 0.098 |
| 0, 1 | **0.083** | **0.101** | 0.084 | 0.080 |
| 0, 2 | 0.032 | 0.038 | 0.015 | 0.020 |
| 0, −1 | 0.010 | 0.011 | 0.074 | 0.072 |
| 0, −2 | | | 0.011 | 0.018 |
| 1, 1 | **0.027** | **0.016** | **0.036** | **0.065** |
| 1, 2 | 0.011 | 0.006 | 0.015 | 0.016 |
| 1, −1 | | | **0.086** | **0.059** |
| 1, −2 | | | 0.023 | 0.015 |

$\phi_1$ and $\phi_2$ cannot be determined correctly on the H-terminated surface using BCF because the pair probabilities are correlated.

One possible mechanism for correlated $P(i,j)$ is the presence of long-range interactions. Previously, we suggested that step–step interactions might be important [32]. But because of the symmetric nature of $P(i,j)$, in particular $P(1,-1) = P(-1,1)$, the step–step interaction between kinks along an edge can be neglected. The fact that only $P(0,1)$, $P(1,1)$, and $P(1,-1)$ are correlated suggests that a kink-step interaction might be responsible for this correlation. Another possible source is steric repulsion between neighboring H atoms. This effect would be larger on $S_B$ steps where H atoms are oriented parallel to the step edge. We need theory that takes into account these correlations to determine which interactions might be important and must be accounted for to solve this mystery.

#### 4.4.2. Maxwell–Boltzmann statistics

We have also examined the relative step energies assuming MB statistics. In the following analysis, a unit cell will represent a particle whose energy is given by its step structure. Since the unit cells (particles) can be labeled, it is proper to employ Maxwell–Boltzmann statistics to determine the energy difference between state $j$ and the chemical potential $\mu$:

$$\varepsilon_j - \mu = -k_B T \ln\left(\frac{n_j}{N}\right), \tag{3}$$

where $n_j$ is the average number of particles in state $j$ and $N$ is total number of particles.

Fig. 10 depicts the relative population of steps as a function of orientation. The most dramatic change after passivation is observed in region III. While clean surfaces in this region are exclusively composed of r-$D_B$ steps, monohydride surfaces are made of a mixture of 4–5 different steps. Similarly, region IV is composed of a large mixture of steps. The change in step distribution as a function of orientation is due to low step formation energy of the n-$D_B$ steps through a wide range of orientations on the monohydride surfaces. The relative energies of all the step structures as a function of orientation are summarized in Table 2 as determine by MB

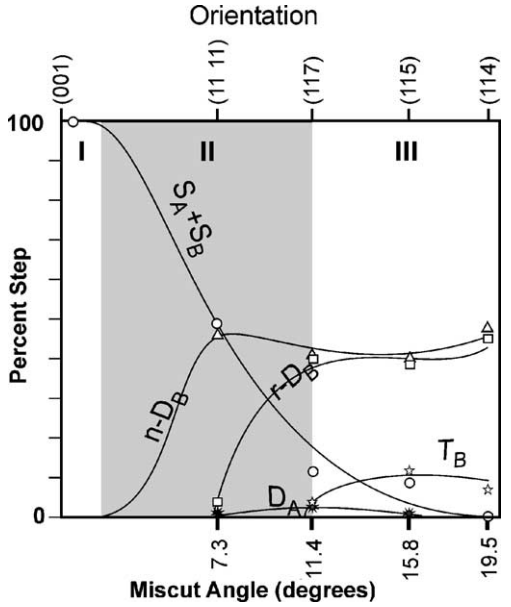


Fig. 10. Distribution of steps on H-terminated vicinal Si(0 0 1). The three regions are defined according to effect that H has on the steps and on the surface morphology. In region I, H roughens the $S_B$ steps. In contrast to region II, where H roughens the surface, H can produced a smoother surface in region III. The lines connecting the symbols are used as a simple guide for the eye.

statistics. It is interesting how the step energy changes as a function of orientation. Whereas the $S_A + S_B$ step energy is lowest on (0 0 1) and increases towards (1 1 4), the n-$D_B$ and r-$D_B$ step energies are larger on (0 0 1), decrease towards (1 1 7), and remain constant towards (1 1 4). In contrast, the $D_A$ and $T_B + S_A$ step energies appear to have a parabolic behavior, with minimum values at (1 1 7) and (1 1 5), respectively.

There has been some theoretical work examining the step-formation energies on H-terminated Si(0 0 1) surfaces [26,45,46]. Zunger, Zhang, and Reboredo have examined the step-formation energies as a function of H chemical potential [45]. Although they did not consider the $T_B + S_A$ steps, their findings are in good qualitative agreement with our results. Their $2\times1$ monohydride phase step energies for $\mu_H \sim -0.75$ agree with our Si(1 1 7), (1 1 5), and (1 1 4) results. For the most part their step energies at $\mu_H \sim -0.5$ agree with what we have observed on Si(1 1 11). The only discrepancy between these results is the offset energy of the n-$S_A$ + n-$S_B$ step. We find that an offset energy of $-0.75$ eV provides the best agreement between their theory and our experiment. It is worth noting that the calculated energy of a $D_A$ step decreases steeply with increasing $\mu_H$, suggesting that $D_A$ steps should have a $(1\times1)$ phase. This prediction could explain the emergence of the $D_A$ steps on Si(1 1 11). Although, we do observe that the $D_A$ step energy decreases with increasing $\mu_H$, at this time we have observed no evidence for dihydride $D_A$ steps.

To further characterize the step energetics on Si(1 1 11), we have analyzed the steps using a three-particle microstate, defined by $[n_{(x-1)}, n_{(x)}, n_{(x+1)}]$, where $n_{(x)} = \{S_A + S_B,\ \text{n-}D_B,\ \text{r-}D_B\}$ represents the type of step at position $x$. After counting the number of microstates, the energy between microstates was determined using Eq. (3). The results are shown schematically in Fig. 11. Although the energy barrier between microstates is completely unknown, it is interesting to note that the energy difference between microstates (n-$D_B$, n-$D_B$, n-$D_B$) and (r-$D_B$, r-$D_B$, r-$D_B$) is almost 2 $k_BT$. This indicates that while it is highly favorable for r-$D_B$ steps to loose their rebonded atoms, it is also unlikely for rebonded atoms to attach to n-$D_B$ steps. A final point to this large energy barrier is that

Table 2
Measured step structure energies $\varepsilon_j$ relative to the surface hydrogen chemical potential $\mu$

| Surface orientation | Relative step structure energies ($\varepsilon_j - \mu$) | | | | |
|---|---|---|---|---|---|
| | $S_A + S_B$ | n-$D_B$ | r-$D_B$ | $D_A$ | $T_B + S_A$ |
| (1 1 11) | 44 ± 4 | 50 ± 4 | 200 ± 10 | 280 ± 20 | |
| (1 1 7) | 130 ± 6 | 55 ± 4 | 60 ± 4 | 220 ± 10 | 200 ± 10 |
| (1 1 5) | 150 ± 6 | 60 ± 3 | 60 ± 3 | 280 ± 20 | 130 ± 5 |
| (1 1 4) | | 45 ± 6 | 50 ± 6 | | 170 ± 10 |

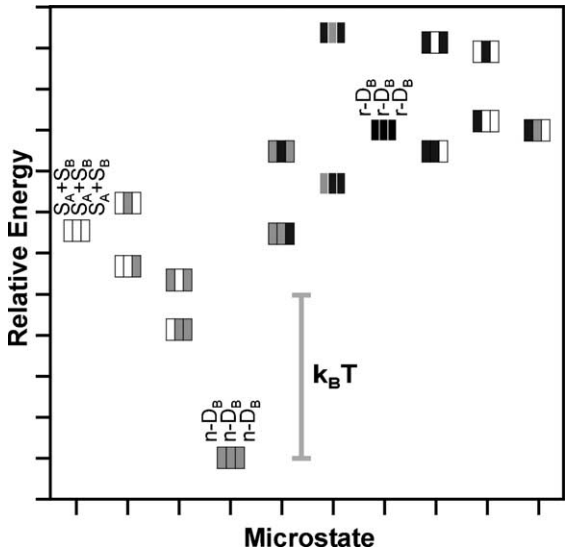


Fig. 11. Relative energy of the microstates in Si(1 1 11) according to Maxwell–Boltzmann statistics. Notice the energy scale of $k_BT$ indicated by the bar. The steps are labeled; $S_A + S_B$ empty rectangles, n-$D_B$ gray rectangles, and r-$D_B$ black rectangles.

rebonded atoms are more likely to desorb from the surface than to diffuse on the surface, in agreement with our previous conclusion.

### 4.5. Hydrogen chemical potential

The effects of $\mu_H$ are most noticeable on Si(1 1 5) and Si(1 1 11). The chemical potential was modified by either changing the surface temperature or by changing the $H_2$ background pressure. On Si(1 1 5) we find a range of $\mu_H$ where the surface roughness has its lowest value. Outside this range the surface either shows signs of pitting, or remains faceted but rougher. The increase in surface roughness is due to etch pits created at the lower surface temperature and is also due to redistribution of the types of steps.

On Si(1 1 11), the step equilibrium structure strongly depends on $\mu_H$. After preparing a monohydride surface that was mostly composed of n-$D_B$ and $S_A + S_B$ steps, the surface was post-annealed without hydrogen (i.e. lower $\mu_H$). Interestingly, the r-$D_B$ steps dominated the resulting surface and there was negligible H desorption. It is somewhat puzzling that the surface undergoes such a structural reconstruction without H present while remaining H passivated. Because mass appears to be conserved, one possible explanation for this restructuring is the detachment and diffusion of H-terminated dimers ($Si_2H_2$) from n-$D_B$ steps to $S_A + S_B$ steps. This process requires the intermediate formation of two dangling bonds, two SiH, and adsorbed $Si_2H_2$ at the n-$D_B$ step. Eventually the adsorbed $Si_2H_2$ reacts with an $S_A + S_B$ step releasing two $H_2$ and forming a r-$D_B$ step. In contrast, exposures at higher H background pressure (i.e. higher $\mu_H$) produced a surface mostly composed of $D_A$ steps. This degree of surface restructuring requires a significant amount of Si ($\sim$0.5 ML) to move in order for the steps to rearrange into $D_A$ steps. The emergence of $D_A$ steps suggests that the $D_A$ steps are stable at higher $\mu_H$, in good agreement with previous theoretical work [45].

## 5. Summary

In summary, we have determined the equilibrium step structures and surface morphologies for the whole range of monohydride-terminated (0 0 1)-terrace-plus-step surfaces. H causes the steps to restructure and alters the energy balance between the various types of steps. The new step distribution produced by H exposure causes the changes in the overall surface morphology, which depends on the H chemical potential. The step restructuring can be accounted for by the removal of rebonded atoms and the diffusion of dimers. Aside from vacancies created by $Si_2H_2$ desorption, no macroscopic etching was observed on the surface. Our analysis indicates that the surfaces are in local equilibrium, and Maxwell–Boltzmann statistics and BCF were employed to determine the relative energies between steps.

Our understanding of the step structure and step energy differences between clean and H-terminated vicinal Si(0 0 1) surfaces can help explain some of the previously reported effects of $H_2$ on film growth. During Si homoepitaxy by either MBE or CVD, hydrogen increases the island density and reduces the island shape anisotropy [7,47]. Although H-termination can decrease the Si adatom diffusion rate [7], these effects can be accounted

for if H somehow "poisons" the $S_B$ step edges, inhibiting Si adatom attachment [48]. Our results provide a simple atomistic explanation. On H-terminated surfaces, the $S_B$ steps are non-rebonded, and attaching a Si adatom to the step edge is tantamount to converting it to a higher-energy rebounded step. This simple mechanism could also account for similar effects of hydrogen on Ge and SiGe film growth [49–51], and may explain the suppression of Co and Ni silicide formation on H-terminated Si [52–54]. Similarly, our results may explain the spontaneous step formation observed on Si(0 0 1) annealed in $H_2$ under extreme conditions ($\sim$1 atm, 1200 °C) [55].

It is important to acknowledge that when hydrogen is present during growth, like in CVD, it completely disrupts the surface morphology on high-index substrates. Therefore, any models based on a simple periodic terrace-plus-step structure are unlikely to be accurate. Although we have focused on the effects of H on film growth, we expect the step edges to be modified in similar ways during the etching of silicon by halogen gases. These are just a few examples of how knowledge of the actual step structures and their energies should prove useful for developing high-fidelity models of silicon growth and processing.

## Acknowledgements

Special thanks to Sarah Bowman for assistance characterizing Si(1 1 5). In addition, the authors thank Steve Hellberg for useful conversations regarding the analysis of the Si(0 0 1) steps.

## References

[1] M. Copel, M.C. Reuter, E. Kaxiras, R.M. Tromp, Phys. Rev. Lett. 63 (1989) 632.
[2] K. Fujita, M. Ichikawa, Appl. Phys. Lett. 73 (1995) 605.
[3] D.E. Jones, J.P. Pelz, Y. Hong, E. Bauer, I.S.T. Tsong, Phys. Rev. Lett. 77 (1996) 330.
[4] R. Hild, C. Seifert, M. Kammler, F.J. Meyer zu Heringdorf, M. Horn-von-Hoegen, R.A. Zhachuk, B.Z. Olshanetsky, Surf. Sci. 512 (2002) 117.
[5] E.D. Williams, N.C. Bartelt, Ultramicroscopy 31 (1989) 36.
[6] J.B. Hannon, J. Tersoff, M.C. Reuter, R.M. Tromp, Phys. Rev. Lett. 89 (2002) 266103.
[7] J.E. Vasek, Z. Zhang, C.T. Salling, M.G. Lagally, Phys. Rev. B 51 (1995) 17207.
[8] S.T. Jemander, H.M. Zhang, R.I.G. Uhrberg, G.V. Hansson, Phys. Rev. B 65 (2002) 115321.
[9] G.H. Cocoletzi, N. Takeuchi, Surf. Sci. 504 (2002) 101.
[10] S.C. Erwin, A.A. Baski, L.J. Whitman, R.E. Rudd, Phys. Rev. Lett. 83 (1999) 1818.
[11] R.M. Tromp, J.B. Hannon, Surf. Rev. Lett. 9 (2002) 1565.
[12] H. Brune, Surf. Sci. Rep. 31 (1998) 125.
[13] C. Dongxue, J.J. Boland, Phys. Rev. B 65 (2002) 165336.
[14] B. Voigtlander, Surf. Sci. Rep. 43 (2001) 127.
[15] M. HornvonHoegen, A. Golla, Phys. Rev. Lett. 76 (1996) 2953.
[16] A.A. Baski, S.C. Erwin, L.J. Whitman, Surf. Sci. 392 (1997) 69.
[17] B.S. Swartzentruber, N. Kitamura, M.G. Lagally, M.B. Webb, Phys. Rev. B 47 (1993) 13432.
[18] D.J. Chadi, Phys. Rev. Lett. 59 (1987) 1691.
[19] K. Oura, V.G. Liftshifts, A.A. Saranin, A.V. Zotov, M. Katayama, Surf. Sci. Rep. 35 (1999) 1.
[20] J.J. Boland, Adv. Phys. 42 (1993) 129.
[21] M. Durr, Z. Hu, A. Biedermann, U. Hofer, T.F. Heinz, Phys. Rev. Lett. 88 (2002) 046104.
[22] M. Durr, Z. Hu, A. Biedermann, U. Hofer, T.F. Heinz, Phys. Rev. B 6312 (2001) 121315.
[23] P. Bratu, K.L. Kompa, U. Hofer, Chem. Phys. Lett. 251 (1996) 1.
[24] M.B. Raschke, U. Hofer, Phys. Rev. B 59 (1999) 2783.
[25] T. Komeda, Y. Kumagai, Phys. Rev. B 58 (1998) 1385.
[26] J.E. Northrup, Phys. Rev. B 44 (1991) 1419.
[27] S. Maruno, H. Iwasaki, K. Horioka, L. Sung-te, S. Nakamura, Phys. Rev. B 27 (1983) 4110.
[28] Y.J. Chabal, K. Raghavachari, Phys. Rev. Lett. 54 (1985) 1055.
[29] S.M. Gates, R.R. Kunz, C.M. Greenlief, Surf. Sci. 207 (1989) 364.
[30] C.C. Cheng, J.T. Yates Jr., Phys. Rev. B 43 (1991) 4041.
[31] A. Dinger, C. Lutterloh, J. Kuppers, Chem. Phys. Lett. 320 (2000) 405.
[32] A. Laracuente, L.J. Whitman, Surf. Sci. 476 (2001) L247.
[33] S.C. Erwin, A.A. Baski, L.J. Whitman, Phys. Rev. Lett. 77 (1996) 687.
[34] J.J. Boland, Phys. Rev. Lett. 67 (1991) 1539.
[35] J.J. Boland, Surf. Sci. 244 (1991) 1.
[36] R.E. Stallcup, J.M. Perez, Phys. Rev. Lett. 86 (2001) 3368.
[37] C.F. Herrmann, D.X. Chen, J.J. Boland, Phys. Rev. Lett. 89 (2002) 096102.
[38] K.S. Nakayama, E. Graugnard, J.H. Weaver, Phys. Rev. Lett. 88 (2002) 125508.
[39] C.F. Herrmann, J.J. Boland, Phys. Rev. Lett. 8711 (2001) 115503.
[40] Y. Gong, D.W. Owens, J.H. Weaver, Phys. Rev. B 53 (1996) 16144.

[41] X.R. Qin, P.R. Norton, Phys. Rev. B 53 (1996) 11100.
[42] W.K. Burton, N. Cabrera, F.C. Frank, Philos. Trans. R. Soc. London Ser. A 243 (1951) 299.
[43] H.J.W. Zandvliet, Rev. Mod. Phys. 72 (2000) 593.
[44] D.R. Bowler, M.G. Bowler, Phys. Rev. B 57 (1998) 15385.
[45] F.A. Reboredo, S.B. Zhang, A. Zunger, Phys. Rev. B 6312 (2001) 125316.
[46] S. Jeong, A. Oshiyama, Phys. Rev. Lett. 81 (1998) 5366.
[47] P.-H. Wu, D.-S. Lin, Phys. Rev. B 57 (1998) 12421.
[48] P. Smilauer, K. Mizushima, D.D. Vvedensky, Phys. Rev. Lett. 81 (1998) 5600.
[49] M. Copel, R.M. Tromp, Appl. Phys. Lett. 58 (1991) 2648.
[50] H. Kim, N. Taylor, T.R. Bramblett, J.E. Greene, J. Appl. Phys. 84 (1998) 6372.
[51] S.-J. Kahng, Y.H. Ha, J.-Y. Park, S. Kim, D.W. Moon, Y. Kuk, Phys. Rev. Lett. 80 (1998) 4931.
[52] K. Ishida, Y. Miura, K. Hirose, S. Harada, T. Narusawa, Appl. Phys. Lett. 82 (2003) 1842.
[53] S. Higai, T. Ohno, Phys. Rev. B 65 (2002) 165309.
[54] M. Yoshimura, I. Ono, K. Ueda, Appl. Surf. Sci. 132 (1998) 276.
[55] L. Zhong, A. Hojo, Y. Matsushita, Y. Aiba, K. Hayashi, R. Takeda, H. Shirai, H. Saito, J. Matsushita, J. Yoshikawa, Phys. Rev. B 54 (1996) R2304.